Geometric Tracking Control of Aerial Robots Based on Centroid Vectoring

Lovro Marković, Antun Ivanović, Marko Car, Matko Orsag, Stjepan Bogdan

***Abstract*— This paper focuses on presenting the concept of geometric tracking control for an unmanned aerial vehicle (UAV) based on variations in center of gravity (CoG). The proposed UAV model has the ability to exploit its dynamic CoG as a means of stabilization and control. A mathematical model of such a system is used as a base for developing the nonlinear geometric tracking controller on the special Euclidean group SE(3). Finally, two unique UAV models, presented with a trajectory tracking problem, are simulated in a realistic simulation environment. Performance of the selected control terms is analyzed based on relevant simulation results.**

I. Introduction

Geometric control concept has previously been applied for classic quadrotor vehicles in [1], [2], [3] set up in plus configuration with their CoG located inside the origin of the UAV body frame. Since a unique type of UAV is considered in this paper its mathematical model differs from aforementioned research. Unlike a standard UAV, whose CoG conicides with its body-fixed frame origin, it utilizes variations in CoG in order to achieve attitude tracking and stability. Essentially, this means that such variations, which would usually be considered a disturbance in the system, could be exploited as a means of controlling the UAV. Since a geometric controller is used in this paper, model dynamics need to be expressed on the SE(3) configuration manifold. It is important to note that unlike traditional quadrotor dynamics, CoG vector $\mathbf{r}_{CoG}$ will also be included in the mathematical model.

One of the ways these variations can be achieved is by implementing the moving mass control concept (MMC)[4] on the standard quadrotor UAV. This includes mounting moving masses on the UAV arms, which offset acts as the control input of the system along with rotor speed variation. This is a novel concept first developed in [5] with attitude control considered in [6]. Up to this point, nonlinear geometric control has not been applied to the moving-mass controlled UAV.

Furthermore, CoG variations are achieved by mounting two manipulators to the UAV, each carrying a payload. In this case position of the payload directly determines any difference in CoG. UAVs endowed with manipulators have previously been studied in [7], [8]. Similar problem has already been presented in [9] where end-effector trajectory tracking of a single mounted 3-DOF manipulator is considered. However, in this paper, along with the different approach in controller synthesis, two 2-DOF manipulators are used, each carrying a payload. The main subject for trajectory tracking is still the UAV, while manipulators are considered as an extension, used only for attitude control.

Therefore, the goal of this paper is to present the appropriate dynamic model for UAVs with variable CoG on the SE(3) configuration manifold, choose control terms based on that model and evaluate controller performance on a predefined trajectory tracking problem using two unique UAV models described previously.

For realistic Gazebo simulations, we use μMORUS UAV, which is a scaled down version of the UAV developed within the MORUS project [11].

The paper is organized as follows. First the general mathematical model will be presented on the SE(3) configuration manifold along with expressions for CoG and moments of inertia. Using that mathematical model, control terms will be chosen such that desirable error dynamics can be obtained. Sufficient stability conditions are presented for the obtained error dynamics. Lastly, two sets of simulations will be conducted using the Gazebo simulator and ROS environment. Both UAVs are compared using the same trajectory tracking problem in order to assess performance of each approach.

II. Mathematical model

A. UAV model

First of all, it is necessary to introduce a fixed inertial reference frame $\{\mathbf{e}_1, \mathbf{e}_2, \mathbf{e}_3\}$ and a body-fixed frame $\{\mathbf{b}_1, \mathbf{b}_2, \mathbf{b}_3\}$. Next, we present a general equation for calculating CoG vector from the origin of the body-fixed frame as follows:

$$\mathbf{r}_{CoG} = \frac{m_b\mathbf{r}_b + \sum_{i=1}^{n} m_i\mathbf{r}_i}{m_b + \sum_{i=1}^{n} m_i} = \frac{\sum_{i=1}^{n} m_i\mathbf{r}_i}{m_t}, \qquad (1)$$

The following terms are defined as:

- $\mathbf{r}_{CoG} \in \mathrm{R}^3$ - CoG with respect to the body-fixed frame
- $\mathbf{r}_i \in \mathrm{R}^3$ - Position of the i-th mass or payload w.r.t. the body-fixed frame

Authors are with Faculty of Electrical and Computer Engineering, University of Zagreb, 10000 Zagreb, Croatia (Antun Ivanović, Marko Car, Tomislav Haus, Matko Orsag, Stjepan Bogdan, Lovro Marković) at fer.hr

- $\mathbf{r}_b \in \mathrm{R}^3$ - Position of UAV body w.r.t. the body-fixed frame. Note that because the body frame origin coincides with the rigid body CoG (without considering the moving masses) this term yields $\mathbf{r}_b = 0_{3x1}$
- $m_b \in \mathbb{R}$ - Mass of the UAV body
- $m_i \in \mathbb{R}$ - Mass of the i-th moving mass or payload
- $m_t \in \mathbb{R}$ - Mass of the whole UAV system

Moment of inertia matrix expressed in the body-fixed frame is defined as follows:

$$\mathrm{J} = \mathrm{J}_b + \sum_{i=1}^{n} \mathrm{J}_i \, , \tag{2}$$

where $\mathrm{J}_b \in \mathbb{R}^3$ is body and $\mathrm{J}_i \in \mathbb{R}^3$ is moment of inertia of some mass element outside the origin of the body-fixed frame. Using the parallel axis theorem, one is able to calculate J_i while knowing moment of inertia around its CoG:

$$\mathrm{J}_i = \mathrm{J}_{i,CoG} + m_i(\mathbf{r}_i^T \cdot \mathbf{r}_i \mathrm{I}_{3\times3} - \mathbf{r}_i \cdot \mathbf{r}_i^T) \tag{3}$$

Now we can express the equations of motion in the inertial frame while taking in consideration CoG vector which is located outside the origin of the body-fixed frame[12].
It is important to note that the changes in moment of inertia and CoG have been omitted in favor of simplicity in equations (5) and (7). The complete model dynamics expressed in the inertial frame are presented in the appendix.

$$\dot{\mathbf{x}} = \mathbf{v} \tag{4}$$

$$m_t\dot{\mathbf{v}} + m_t g\mathbf{e}_3 - m_t \mathrm{R}\mathbf{r}_{CoG} \times \dot{\mathbf{\Omega}} - m_t \mathrm{R}\hat{\mathbf{\Omega}}\hat{\mathbf{r}}_{CoG}\mathbf{\Omega} = f\mathrm{R}\mathbf{e}_3 \tag{5}$$

$$\dot{\mathrm{R}} = \mathrm{R}\hat{\mathbf{\Omega}} \tag{6}$$

$$\mathrm{J}\dot{\mathbf{\Omega}} + \mathbf{\Omega} \times \mathrm{J}\mathbf{\Omega} + m_t\mathbf{r}_{CoG} \times \mathrm{R}^T\dot{\mathbf{v}} = \mathbf{M} \tag{7}$$

The *hat map* is an operator equivalent to the expression $\hat{\mathbf{x}}\mathbf{y} = \mathbf{x} \times \mathbf{y}$. It maps elements of $\mathbb{R}^3$ to the so(3) Lie algebra.
The following terms are defined as:

- $\mathrm{J} \in \mathbb{R}^{3\times3}$ - Moment of inertia matrix w.r.t. the body-fixed frame
- $\mathrm{R} \in SO(3)$ - Rotation matrix from the body fixed frame to the inertial frame
- $\mathbf{\Omega} \in \mathbb{R}^3$ - Angular velocity in the body-fixed frame
- $\mathbf{x} \in \mathbb{R}^3$ - Location of the body-fixed frame in the inertial frame
- $\mathbf{v} \in \mathbb{R}^3$ - Velocity of the body-fixed frame in the inertial frame
- $f \in \mathbb{R}$ - Total thrust produced by the UAV
- $\mathbf{M} \in \mathbb{R}^3$ - Total moments acting in the body-fixed frame

Equations (4), (5), (6) and (7) describe the dynamical flow of a rotating and translating rigid body in terms of evolution of $(\mathrm{R}, \mathbf{x}, \mathbf{\Omega}, \dot{\mathbf{x}}) \in \mathrm{TSE}(3)$ on the tangent bundle of SE(3).

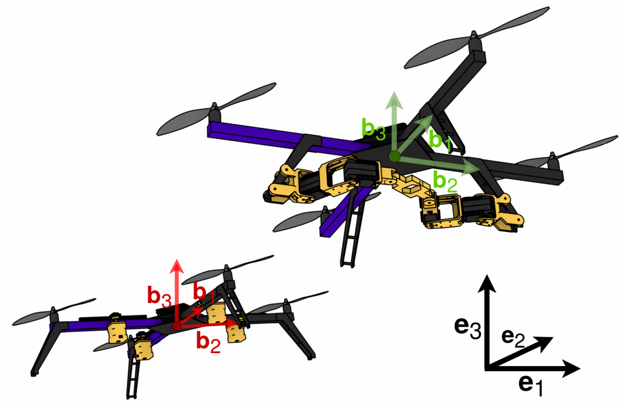

Fig. 1: UAV model with MMC (left) and two 2-DOF overactuated manipulators (right) along with their respective coordinate systems. The manipulator end effectors are placed diametrically opposite from each other.

B. Control inputs

Height and yaw of the UAV is controlled by variations in rotor velocity, whereas roll and pitch by variations in CoG. It is assumed that first and third propeller rotate clockwise, while second and fourth rotate counter-clockwise. The relation between moments, thrust and rotor velocity is the following:

$$f_i = b_f \omega_i^2 \tag{8}$$

$$\tau_i = (-1)^i b_m f_i \, , \tag{9}$$

where the following terms are defined as:

- $f_i \in \mathbb{R}$ - Thrust of the i-th motor
- $\tau_i \in \mathbb{R}$ - Moment i-th motor produces
- $b_f \in \mathbb{R}$ - Motor thrust constant
- $b_m \in \mathbb{R}$ - Motor moment constant
- $\omega_i \in \mathbb{R}$ - Rotation velocity of the i-th rotor

Total thrust can be expressed as:

$$f = \sum_{1}^{4} f_i \, , \tag{10}$$

and total moment acting in the body-fixed frame as:

$$\begin{aligned}\mathbf{M} = [&m_p g d_x \mathbf{e}_1 \cdot \mathbf{b}_{3,d},\\ &m_p g d_y \mathbf{e}_2 \cdot \mathbf{b}_{3,d},\\ &b_m(-f_1 + f_2 - f_3 + f_4)] \, ,\end{aligned} \tag{11}$$

where $d_x \in \mathbb{R}$ and $d_y \in \mathbb{R}$ are moving mass or payload offsets along x and y axis respectively.
Using (10) and (11) as control inputs of the system one is able to obtain the desired force of each rotor and the control offset d_x and d_y. While the control offsets are able to be directly applied as moving mass control inputs,

in the manipulator case they need to be converted to infinitesimal actuator angle increments $\Delta q_1, \Delta q_2, \Delta q_3$. Such conversion is done using the inverse Jacobian of the manipulator end effector.
Direct Jacobian matrix is presented as follows:

$$\begin{bmatrix} d_x \\ d_y \end{bmatrix} = \mathcal{J}(q_1, q_2, q_3) \cdot \begin{bmatrix} \Delta q_1 \\ \Delta q_2 \\ \Delta q_3 \end{bmatrix} \tag{12}$$

$$\mathcal{J} = \begin{bmatrix} l_1\cos(q_1) & l_2\cos(q_1+q_2) & l_3\cos(q_1+q_2+q_3) \\ l_1\sin(q_1) & l_2\sin(q_1+q_2) & l_3\sin(q_1+q_2+q_3) \end{bmatrix}, \tag{13}$$

where l_1, l_2 and l_3 are the manipulator link lengths, while q_1, q_2 and q_3 are current actuator angles. Using Jacobian pseudinverse, incremental update rule for actuator angles can be obtained as follows:

$$\begin{bmatrix} \Delta q_1 \\ \Delta q_2 \\ \Delta q_3 \end{bmatrix} = \mathcal{J}^{-1}(q_1, q_2, q_3) \cdot \begin{bmatrix} d_x \\ d_y \end{bmatrix} \tag{14}$$

Manipulator and moving mass actuator dynamics along with the change in desired rotor force will be regarded as instantaneous while presenting the controller synthesis and stability conditions. However, within the Gazebo simulation environment, a certain transfer dynamic is taken in account.

III. Geometric control on SE(3)

In this section a nonlinear tracking controller will be developed. The main focus will be put on position tracking, therefore the trajectory will consist of a desired position $\mathbf{x}_d(t)$ and desired heading $\mathbf{b}_{1,d}$ of the body-fixed frame. Since the given position is known ahead of time, one is able to calculate both desired linear velocity $\mathbf{v}_d(t)$ and acceleration $\mathbf{a}_d(t)$ which will also inherently be included as inputs.
The controller will be developed on the nonlinear Lie group SE(3) whose subgroups are the rotation group SO(3) and translation group T(3). The main advantage of using the SO(3) rotation group is to avoid any singularities or ambiguities that may arise when representing rotations with Euler angles or quaternions.
Firstly, chosen position and orientation errors will be presented which will also lie on the SE(3) manifold and its tangent space. Using previously defined errors, nonlinear control terms can be chosen. Finally, the stability conditions of the tracking errors will be presented.

A. Tracking errors

Compatible attitude error function and transport map between tangent bundles of SO(3) are chosen as suggested in [13] and confirmed in research regarding geometric control with aerial vehicles [3], [10], [2], [1]. Attitude error function on SO(3) along with its compatible transport map are chosen as:

$$\Psi(\mathrm{R}, \mathrm{R}_d) = \frac{1}{2} tr[I - \mathrm{R}_d^T \mathrm{R}] \tag{15}$$

$$\mathcal{T}(\mathrm{R}, \mathrm{R}_d) = \mathrm{R}^T \mathrm{R}_d \tag{16}$$

Linear position and velocity tracking errors are defined as follows:

$$\mathbf{e}_x = \mathbf{x} - \mathbf{x}_d \tag{17}$$

$$\mathbf{e}_v = \mathbf{v} - \mathbf{v}_d \tag{18}$$

Defining attitude and angular velocity tracking errors is not as straight-forward. It is shown in [13] that the attitude tracking error should be chosen as a left-differential of the attitude error function $\Psi(\mathrm{R}, \mathrm{R}_d)$. It is chosen as follows:

$$\mathbf{e}_{\mathrm{R}} = \frac{1}{2}(\mathrm{R}_d^T \mathrm{R} - \mathrm{R}^T \mathrm{R}_d)^{\vee} \tag{19}$$

Due to the fact that angular velocities $\mathbf{\Omega} \in T_{\mathrm{R}} SO(3)$ and $\mathbf{\Omega}_d \in T_{\mathrm{R}_d} SO(3)$ lie in different tangential bundles, the proposed left transport map 16 needs to be applied when calculating the tracking error:

$$\mathbf{e}_{\Omega} = \mathbf{\Omega} - \mathrm{R}^T \mathrm{R}_d \mathbf{\Omega}_d \tag{20}$$

B. Control terms

Taking in consideration the proposed system dynamics 5 and 7, the force and moment control terms are chosen as follows:

$$\begin{aligned} \mathbf{A} = (&-\mathrm{k}_x \mathbf{e}_x - \mathrm{k}_v \mathbf{e}_v \\ &+ mg\mathbf{e}_3 + m\ddot{\mathbf{x}}_d \\ &- m\mathrm{R}\mathbf{r}_{CoG} \times \dot{\mathbf{\Omega}} - m\mathrm{R}\hat{\mathbf{\Omega}}\hat{\mathbf{r}}_{CoG}\mathbf{\Omega}) \\ f =& \mathbf{A} \cdot \mathrm{R}\mathbf{e}_3 \end{aligned} \tag{21}$$

$$\begin{aligned} \mathbf{M} = &-\mathrm{k}_{\mathrm{R}} \mathbf{e}_{\mathrm{R}} - \mathrm{k}_{\Omega} \mathbf{e}_{\Omega} \\ &+ \mathbf{\Omega} \times \mathrm{J}\mathbf{\Omega} - \mathrm{J}(\hat{\mathbf{\Omega}} \mathrm{R}^T \mathrm{R}_d \mathbf{\Omega}_d - \mathrm{R}^T \mathrm{R}_d \dot{\mathbf{\Omega}}_d) \\ &+ m\mathbf{r}_{CoG} \times \mathrm{R}^T \ddot{\mathbf{x}} \end{aligned} \tag{22}$$

When error dynamics will be presented, it can be seen that the control terms are chosen in order to negate the undesirable system dynamics.

Desired rotation matrix is constructed in the traditional way when considering geometric control of aerial vehicles [1], [2], [10]. The proposed desired rotation matrix is constructed as $\mathrm{R}_d = [\mathbf{b}_{1,c}, \mathbf{b}_{3,d} \times \mathbf{b}_{1,c}, \mathbf{b}_{3,d}]$ where component vectors of R_d are calculated in the following way:

$$\mathbf{b}_{3,d} = \frac{\mathbf{A}}{||\mathbf{A}||} \tag{23}$$

$$\mathbf{b}_{1,c} = -\frac{(\mathbf{b}_{3,d} \times (\mathbf{b}_{3,d} \times \mathbf{b}_{1,d}))}{||\mathbf{b}_{3,d} \times \mathbf{b}_{1,d}||} \tag{24}$$

It is also assumed that:

$$||\mathbf{A}|| \neq 0 \tag{25}$$

The chosen constraint for the trajectory tracking problem differs slightly from the one proposed in [1] due to the fact that different model dynamics are considered in this paper. New trajectory constraints are presented as follows:

$$||mge_3 + m\ddot{\mathbf{x}}_d - m\mathrm{R}\mathbf{r}_{CoG} \times \dot{\mathbf{\Omega}} - m\mathrm{R}\hat{\mathbf{\Omega}}\hat{\mathbf{r}}_{CoG}\mathbf{\Omega}|| < B \tag{26}$$

where B is some positive constant.

Desired angular velocity and acceleration also need to be considered in this trajectory tracking problem. One is able to calculate the desired angular velocity and acceleration using R_d and its derivatives in the following way:

$$\hat{\mathbf{\Omega}}_d = \mathrm{R}_d^T \dot{\mathrm{R}}_d \tag{27}$$

$$\dot{\hat{\mathbf{\Omega}}}_d = -\hat{\mathbf{\Omega}}_d \hat{\mathbf{\Omega}}_d + \mathrm{R}_d^T \ddot{\mathrm{R}}_d \tag{28}$$

Derivatives of R_d are easily calculated using the backwards differentiation method. It has to be noted that due to stability issues, computation rate of desired angular velocity and acceleration has to be lesser than the overall simulation rate. For further implementation details, please refer to [14].

C. Error dynamics and stability discussion

In this section linear and angular error dynamics will be presented. First of all, derivatives over time need to be calculated for linear 18 and angular 20 tracking errors:

$$\mathbf{e}_v = \dot{\mathbf{x}} - \dot{\mathbf{x}}_d \tag{29}$$

$$\mathbf{e}_\Omega = \dot{\mathbf{\Omega}} + \hat{\mathbf{\Omega}}\mathrm{R}^T\mathrm{R}_d\mathbf{\Omega}_d - \mathrm{R}^T\mathrm{R}_d\dot{\mathbf{\Omega}}_d \tag{30}$$

After including 5 and 7 in 29 and 30 respectively, the following equations are obtained:

$$\begin{aligned} m\mathbf{e}_v =& -mg\mathbf{e}_3 - m\ddot{\mathbf{x}}_d \\ &+ m\mathrm{R}\mathbf{r}_{CoG} \times \dot{\mathbf{\Omega}} + m\mathrm{R}\hat{\mathbf{\Omega}}\hat{\mathbf{r}}_{CoG}\mathbf{\Omega} \qquad (31) \\ &+ \mathbf{A} + \mathbf{X} \end{aligned}$$

$$\begin{aligned} \mathrm{J}\mathbf{e}_\Omega =& \mathbf{M} - \mathbf{\Omega} \times \mathrm{J}\mathbf{\Omega} \\ &+ \mathrm{J}(\hat{\mathbf{\Omega}}\mathrm{R}^T\mathrm{R}_d\mathbf{\Omega}_d - \mathrm{R}^T\mathrm{R}_d\dot{\mathbf{\Omega}}_d) \qquad (32) \\ &+ m\mathbf{r}_{CoG} \times \mathrm{R}^T\ddot{\mathbf{x}} \end{aligned}$$

Note that in 31 $\mathbf{A} \in \mathrm{R}^3$ is regarded as a control force for the translational dynamics, mentioned in 21, while $\mathbf{X} \in \mathrm{R}^3$ is a bounded term that arises when deriving this equation which equals:

$$\mathbf{X} = \frac{f}{(\mathrm{R}_d\mathbf{e}_3)^T\mathrm{R}\mathbf{e}_3}(\mathrm{R}_d\mathbf{e}_3 - ((\mathrm{R}_d\mathbf{e}_3)^T\mathrm{R}\mathbf{e}_3)\mathrm{R}\mathbf{e}_3) \tag{33}$$

After substituting control force from 21 and 22 in 31 and 32 respectively the final form of error dynamics is

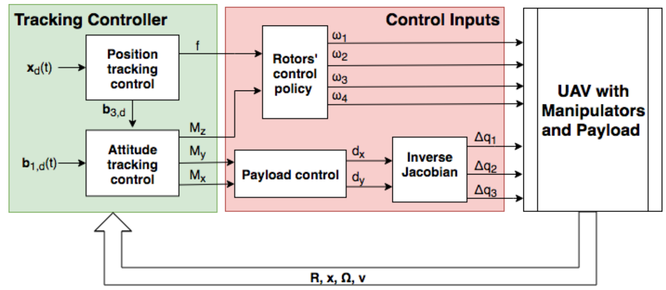

Fig. 2: Control scheme for the case of UAV carrying the payload. It is important to note that for the case of UAV with moving masses, *Inverse Jacobian* block will be omitted and control inputs d_x and d_y will be directly sent to the moving mass actuators.

obtained:

$$m\mathbf{e}_v = -k_x\mathbf{e}_x - k_v\mathbf{e}_v + \mathbf{X} \tag{34}$$

$$\mathrm{J}\mathbf{e}_\Omega = -k_\mathrm{R}\mathbf{e}_\mathrm{R} - \mathrm{k}_\Omega\mathbf{e}_\Omega \tag{35}$$

Having started with a different mathematical model of the UAV than the previous research done on this subject, applying the newly formed control terms 21 and 22 and taking in consideration initial assumptions 25 and 26 one is able to derive identical translational and rotational error dynamics as found in [3], [1].
Therefore, to avoid redundancy, the full stability proof will not be presented in this paper. However, the final conclusions for exponential asymptotic stability of the attitude error function and attraction to the zero-equilibrium state of tracking errors will be outlined.

If the initial UAV configuration satisfies the following conditions:

$$\Psi(\mathrm{R}(0), \mathrm{R}_d(0)) < 2 \tag{36}$$

$$||\mathbf{e}_\Omega(0)||^2 < \frac{2}{\lambda_{min}(\mathrm{J})}k_\mathrm{R}(2 - \Psi(\mathrm{R}(0), \mathrm{R}_d(0)) \tag{37}$$

it can be shown that tracking errors of the whole system will reach zero-equilibrium state and the attitude function will be exponentially bounded as:

$$\Psi(\mathrm{R}(t), \mathrm{R}_d(t)) \leq \min\{2, \alpha e^{-\beta t}\} \tag{38}$$

for some positive constants α and β.

IV. Simulation

In this section simulation results will be presented and analysed. Simulations are conducted in the Gazebo simulator within the ROS environment. UAV used in experiments is the μMorus which can be found in the *mmuav_gazebo* repository [14], along with its parameters. Two experiments will be conducted with different methods of CoG variation:

- UAV control based on moving masses

- UAV control based on payload carried by manipulator arms

Control parameters for the first case are chosen as follows:

$$
\mathrm{k}_x = \begin{bmatrix} 10 & 0 & 0 \\ 0 & 10 & 0 \\ 0 & 0 & 50 \end{bmatrix}, \ \mathrm{k}_v = \begin{bmatrix} 3.75 & 0 & 0 \\ 0 & 3.75 & 0 \\ 0 & 0 & 20 \end{bmatrix}
$$

$$
\mathrm{k}_R = \begin{bmatrix} 1.5 & 0 & 0 \\ 0 & 1.5 & 0 \\ 0 & 0 & 10 \end{bmatrix}, \ \mathrm{k}_\Omega = \begin{bmatrix} 0.65 & 0 & 0 \\ 0 & 0.65 & 0 \\ 0 & 0 & 1.54 \end{bmatrix}
$$

Rotational control parameters, in the second case, stay the same, while translational parameters are the following:

$$
\mathrm{k}_x = \begin{bmatrix} 6 & 0 & 0 \\ 0 & 6 & 0 \\ 0 & 0 & 50 \end{bmatrix}, \ \mathrm{k}_v = \begin{bmatrix} 2.5 & 0 & 0 \\ 0 & 2.5 & 0 \\ 0 & 0 & 20 \end{bmatrix}
$$

For both cases, initial parameters are obtained by considering the error dynamics 34 and 35 in the equilibrium state. However, they are further tuned for better performance.

It is important to note that the actuator dynamics of the moving masses is taken in consideration within the Gazebo simulation environment. Furthermore there is a slight transient delay when increasing or decreasing rotor velocity which results in a non-instantaneous control force change. These phenomena were not taken in consideration while modeling the system and choosing control terms.

The chosen trajectory tracking problem is formulated as a rotating spiral:

$$
\mathbf{x}_d(t) = [0.4\mathrm{t};\ 0.5\sin(\pi\mathrm{t});\ 0.6\cos(\pi\mathrm{t}) + 2]
$$
$$
\mathbf{b}_{1,d}(t) = \left[\cos\left(\frac{\pi}{5}\mathrm{t}\right);\ \sin\left(\frac{\pi}{5}\mathrm{t}\right);\ 0\right]
$$

In the first case the total trajectory time is 20s while in the second case it will last 30s. Initial position and orientation is chosen at the start of the trajectory.

V. Conclusion

Geometric control was presented and implemented for two separate UAV models with variable centers of gravity. Although the controller has been constructed without actuator dynamics in mind, during the simulations its effect can be seen. Trajectory problem given to the manipulator controlled UAV had to be somewhat slower in order to be successfully completed. Even still, worse performance can be observed in manipulator controlled UAV 6 compared to the moving mass UAV 3. The main reason for such behavior is the considerably slower actuator dynamics for mounted manipulators. As a result the carried payload will produce much slower change in center of gravity than moving masses.

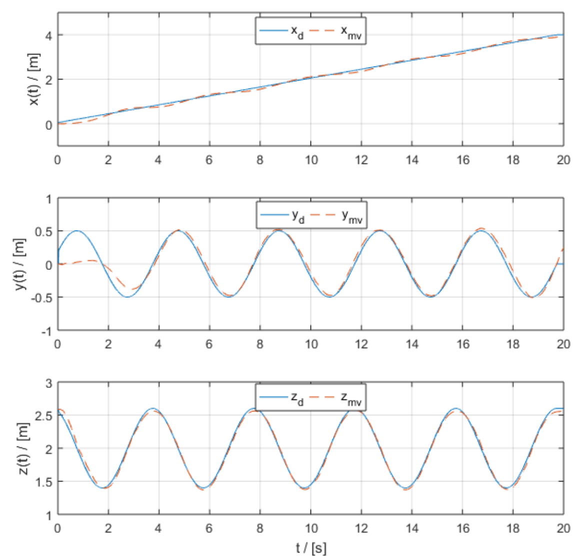

Fig. 3: Comparison of the desired $\mathbf{x}_d$ and measured position values $\mathbf{x}_{mv}$. (Using the moving mass control concept.)

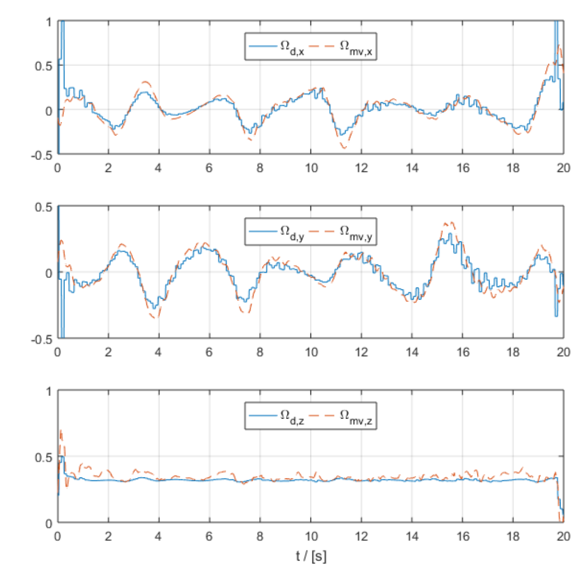

Fig. 4: Comparison of desired $\mathbf{\Omega}_d$ and measured $\mathbf{\Omega}_{mv}$ angular velocity values. (Using the moving mass control concept.)

The overall effect of control terms 21 and 22 which include $\mathbf{r}_{CoG}$ becomes negligible if considering slower trajectories. In such cases, both UAVs can be observed as having CoG inside the origin of the body-fixed frame yielding simpler control terms.

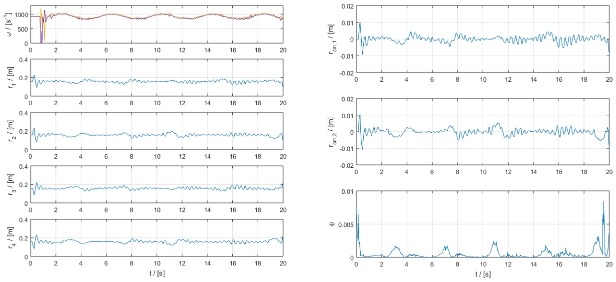

a) b)

Fig. 5: Control inputs are shown in figure a) in the following order: rotor velocities ω_i and mass offsets r_i. Figure b) shows first two components of CoG vector $\mathbf{r}_{CoG}$ (third component is always zero since masses only move in x-y plane of the body-fixed frame) and attitude error function Ψ. (Using the moving mass control concept.)

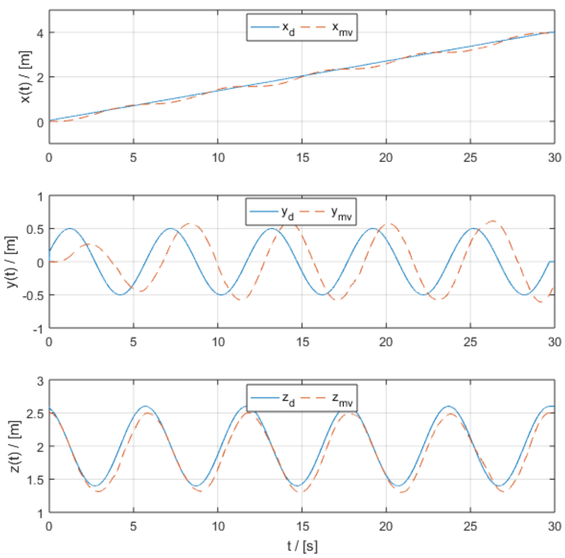

Fig. 6: Comparison of the desired $\mathbf{x}_d$ and measured position values $\mathbf{x}_{mv}$. (Using the manipulator control control.)

APPENDIX

In this section rotating body dynamics with variations in center of gravity will be derived. General form of Euler-Lagrange dynamics for a rotating rigid body in SE(3) configuration manifold in the body-fixed frame as presented in [12]:

$$\frac{d}{dt}\left(\frac{\partial \mathcal{L}}{\partial \boldsymbol{\Omega}}\right) + \boldsymbol{\Omega} \times \frac{\partial \mathcal{L}}{\partial \boldsymbol{\Omega}} + \mathbf{v} \times \frac{\partial \mathcal{L}}{\partial \mathbf{v}} + \sum_{i=1}^{3} \mathbf{r}_i \times \frac{\partial \mathcal{L}}{\partial \mathbf{r}_i} = 0 \tag{39}$$

$$\frac{d}{dt}\left(\frac{\partial \mathcal{L}}{\partial \mathbf{v}}\right) + \boldsymbol{\Omega} \times \frac{\partial \mathcal{L}}{\partial \mathbf{v}} - \mathrm{R}^T \frac{\partial \mathcal{L}}{\partial x} = 0 \tag{40}$$

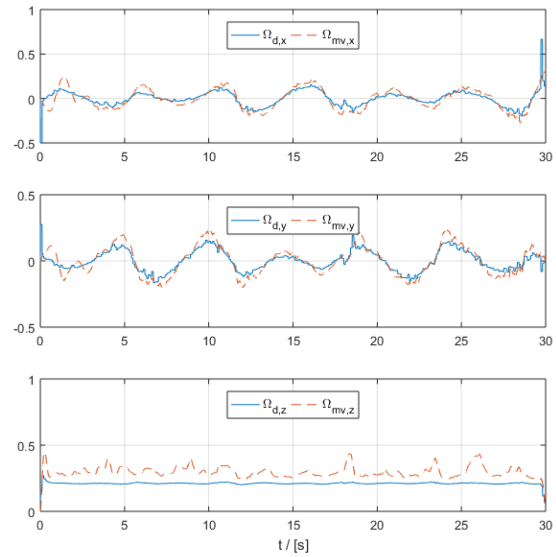

Fig. 7: Comparison of desired $\boldsymbol{\Omega}_d$ and measured $\boldsymbol{\Omega}_{mv}$ angular velocity values. (Using the manipulator control concept)

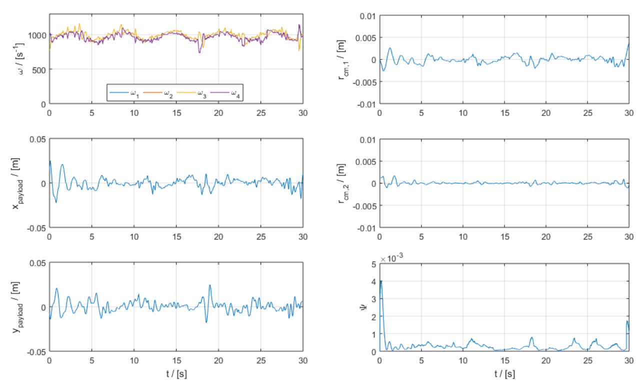

a) b)

Fig. 8: Control inputs: rotor velocities ω_i and payload position; are shown in in figure a). Figure b) shows first two components of CoG vector $\mathbf{r}_{CoG}$ and attitude error function Ψ.

For the the proposed UAS with variations in center of mass the Lagrangian is:

$$\mathcal{L}(\mathrm{R}, x, \boldsymbol{\Omega}, \mathbf{v}) = \frac{1}{2}\boldsymbol{\Omega}^T J \boldsymbol{\Omega} + m\boldsymbol{\Omega}^T \hat{\mathbf{r}}_{cm}\mathbf{v} + \frac{1}{2} m \mathbf{v}^T \mathbf{v} - U(\mathrm{R}, \mathbf{x}) \tag{41}$$

where $U(\mathrm{R}, \mathbf{x})$ is the potential energy of the system. It is important to note that J and $\mathbf{r}_{cm}$ are variable over time. Lagrangian derivatives needed for the general form equations 39 and 40 are:

$$\frac{\partial \mathcal{L}}{\partial \mathbf{\Omega}} = J\mathbf{\Omega} + m\hat{\mathbf{r}}_{cm})\mathbf{v} \tag{42}$$

$$\frac{d}{dt}\left(\frac{\partial \mathcal{L}}{\partial \mathbf{\Omega}}\right) = \dot{J}\mathbf{\Omega} + J\dot{\mathbf{\Omega}} + m\dot{\mathbf{r}}_{cm} \times \mathbf{v} + m\mathbf{r}_{cm} \times \dot{\mathbf{v}} \tag{43}$$

$$\frac{\partial \mathcal{L}}{\partial \mathbf{v}} = m\mathbf{v} - m\mathbf{r}_{cm} \times \mathbf{\Omega} \tag{44}$$

$$\frac{d}{dt}\left(\frac{\partial \mathcal{L}}{\partial \mathbf{v}}\right) = m\dot{\mathbf{v}} - m\dot{\mathbf{r}}_{cm} \times \mathbf{\Omega} - m\mathbf{r}_{cm} \times \dot{\mathbf{\Omega}} \tag{45}$$

It is of interest to transfer rotation and translation dynamics in the inertial frame. This can be done using the following relations:

$$\mathbf{v} = \mathrm{R}^T\dot{x} \tag{46}$$

$$\dot{\mathbf{v}} = \mathrm{R}^T\ddot{\mathbf{x}} - \mathbf{\Omega} \times (\mathrm{R}^T\dot{\mathbf{x}}) \tag{47}$$

$$\mathbf{r}_{cm} = \mathrm{R}^T(\mathbf{x}_{cm} - \mathbf{x}) \tag{48}$$

$$\dot{\mathbf{r}}_{cm} = \mathrm{R}^T(\dot{\mathbf{x}}_{cm} - \dot{\mathbf{x}}) + \mathrm{R}^T\hat{\mathbf{\Omega}}\mathbf{x}_{cm} - \hat{\mathbf{\Omega}}\mathrm{R}^T(\mathbf{x}_{cm} - \mathbf{x}) \tag{49}$$

After plugging in 42, 43, 44, 45 in 39, 40 and using 46, 47 as transformations of velocity and acceleration to inertial frame the following equations are obtained:

$$\begin{aligned} &J\dot{\mathbf{\Omega}} + m\mathbf{r}_{cm} \times \mathrm{R}^T\ddot{\mathbf{x}} \\ &+ \dot{J}\mathbf{\Omega} + m\dot{\mathbf{r}}_{cm} \times \mathrm{R}^T\dot{\mathbf{x}} \\ &+ \mathbf{\Omega} \times J\mathbf{\Omega} + \sum_{i=1}^{3} \mathbf{r}_i \times \frac{\partial \mathcal{L}}{\partial \mathbf{r}_i} = 0 \end{aligned} \tag{50}$$

$$\begin{aligned} &m\ddot{\mathbf{x}} - m\mathrm{R}\hat{\mathbf{r}}_{cm}\dot{\mathbf{\Omega}} - m\mathrm{R}\hat{\dot{\mathbf{r}}}_{cm}\mathbf{\Omega} \\ &- m\mathrm{R}\hat{\mathbf{\Omega}}\hat{\mathbf{r}}_{cm}\mathbf{\Omega} + \frac{\partial U(\mathrm{R}, \mathbf{x})}{\partial \mathbf{x}} = 0 \end{aligned} \tag{51}$$

After plugging in the center of mass transform 48, 49 the final form of dynamics is obtained:

$$\begin{aligned} &J\dot{\mathbf{\Omega}} + m\mathrm{R}^T(\mathbf{x}_{cm} - \mathbf{x}) \times \mathrm{R}^T\ddot{\mathbf{x}} + \dot{J}\mathbf{\Omega} \\ &+ m\widehat{\mathrm{R}^T\dot{\mathbf{x}}_{cm}}\mathrm{R}^T\dot{\mathbf{x}} - \mathrm{R}^T\dot{\mathbf{x}} \times (\mathrm{R}^T\hat{\mathbf{\Omega}}\mathbf{x}_{cm}) \\ &- m\hat{\mathbf{\Omega}}\mathrm{R}^T(\mathbf{x}_{cm} - \mathbf{x}) \times \mathrm{R}^T\dot{\mathbf{x}} \\ &+ \mathbf{\Omega} \times J\mathbf{\Omega} + \sum_{i=1}^{3} \mathbf{r}_i \times \frac{\partial \mathcal{L}}{\partial \mathbf{r}_i} = 0 \end{aligned} \tag{52}$$

$$\begin{aligned} &m\ddot{\mathbf{x}} - m\mathrm{R}\widehat{\mathrm{R}^T(\mathbf{x}_{cm} - \mathbf{x})}\dot{\mathbf{\Omega}} \\ &- m\mathrm{R}\widehat{\mathrm{R}^T(\dot{\mathbf{x}}_{cm} - \dot{\mathbf{x}})}\mathbf{\Omega} \\ &- m\mathrm{R}\widehat{\mathrm{R}^T\hat{\mathbf{\Omega}}\mathbf{x}_{cm}}\mathbf{\Omega} \\ &+ \frac{\partial U(\mathrm{R}, \mathbf{x})}{\partial \mathbf{x}} = 0 \end{aligned} \tag{53}$$

ACKNOWLEDGMENT

This research was supported in part by NATO's Emerging Security Challenges Division in the framework of the Science for Peace and Security Programme as Multi Year Project under G. A. number 984807, named Unmanned system for maritime security and environmental monitoring - MORUS.

References

[1] T. Lee, M. Leok, and N. H. McClamroch, "Geometric tracking control of a quadrotor uav on se(3)," in *49th IEEE Conference on Decision and Control (CDC)*, pp. 5420–5425, Dec 2010.

[2] T. Lee, M. Leok, and N. Harris McClamroch, "Nonlinear Robust Tracking Control of a Quadrotor UAV on SE(3)," *ArXiv e-prints*, Sept. 2011.

[3] T. Lee, M. Leok, and N. Harris McClamroch, "Control of Complex Maneuvers for a Quadrotor UAV using Geometric Methods on SE(3)," *ArXiv e-prints*, Mar. 2010.

[4] T. Haus, M. Orsag, and S. Bogdan, "Design considerations for a large quadrotor with moving mass control," in *2016 International Conference on Unmanned Aircraft Systems (ICUAS)*, pp. 1327–1334, June 2016.

[5] T. Haus, M. Orsag, and S. Bogdan, "Mathematical modelling and control of an unmanned aerial vehicle with moving mass control concept," *Journal of Intelligent & Robotic Systems*, vol. 88, pp. 219–246, Dec 2017.

[6] T. Haus, N. Prkut, K. Borovina, B. Marić, M. Orsag, and S. Bogdan, "A novel concept of attitude control for large multirotor-uavs based on moving mass control," in *2016 24th Mediterranean Conference on Control and Automation (MED)*, pp. 832–839, June 2016.

[7] M. Orsag, C. Korpela, S. Bogdan, and P. Oh, "Dexterous aerial robots—mobile manipulation using unmanned aerial systems," *IEEE Transactions on Robotics*, vol. 33, pp. 1453–1466, Dec 2017.

[8] C. Korpela, M. Orsag, M. Pekala, and P. Oh, "Dynamic stability of a mobile manipulating unmanned aerial vehicle," in *2013 IEEE International Conference on Robotics and Automation*, pp. 4922–4927, May 2013.

[9] H. Yang and D. Lee, "Dynamics and control of quadrotor with robotic manipulator," in *2014 IEEE International Conference on Robotics and Automation (ICRA)*, pp. 5544–5549, May 2014.

[10] T. Fernando, J. Chandiramani, T. Lee, and H. Gutierrez, "Robust adaptive geometric tracking controls on so(3) with an application to the attitude dynamics of a quadrotor uav," in *2011 50th IEEE Conference on Decision and Control and European Control Conference*, pp. 7380–7385, Dec 2011.

[11] "Morus project." `http://www.fer.unizg.hr/morus`. Accessed: 2017-09-08.

[12] T. Lee, M. Leok, and N. H. McClamroch, *Global formulations of Lagrangian and Hamiltonian dynamics on manifolds : a geometric approach to modeling and analysis*. Interaction of mechanics and mathematics series, Springer, 2018.

[13] A. D. L. Francesco Bullo, *Geometric control of mechanical systems: modeling, analysis, and design for simple mechanical control systems*. Texts in applied mathematics 49, Springer, 1 ed., 2005.

[14] "mmuav gazebo." `https://github.com/larics/mmuav_gazebo/tree/geometry_control`, 2018.

[15] A. D. L. Francesco Bullo, *Geometric control of mechanical systems: modeling, analysis, and design for simple mechanical control systems*. Texts in applied mathematics 49, Springer, 1 ed., 2005.

[16] F. P. Schuller, *Lectures on the Geometric Anatomy of Theoretical Physics*. Friedrich-Alexander-Universität Erlangen-Nürnberg, Institut für Theoretische Physik III, 2017.